

Site-directed Mutagenesis and HPLC Analysis of Inosine-Uridine Nucleoside Hydrolase  
RihC of *Escherichia coli*

by

Brock A. Arivett

A Thesis Submitted in Partial Fulfillment  
of the Requirements for the Degree of  
Master of Science in Biology

Middle Tennessee State University  
December 2014

Thesis Committee:

Dr. Mary B. Farone, Chair

Dr. Anthony L. Farone

Dr. Paul C. Kline

I dedicate this to the memories of Bonnie Howard, Shirley Arivett, and Rosie Collins.

## **ACKNOWLEDGEMENTS**

I am delighted to thank my wife, Deanna. Her love and encouragement have made this possible. I am grateful for the support given by everyone in our family.

## ABSTRACT

Recycling of purine and pyrimidine bases is critical in the metabolism of many organisms. While the archetype enzyme, Inosine-Uridine Nucleoside Hydrolase (IU-NH) of *Crithidia fasciculata*, is well studied because of its potential as a therapeutic target, other enzymes have not been well characterized, including ribonucleoside hydrolase C (RihC) of *Escherichia coli*. This study examined the effects of amino acid changes at conserved residues of RihC that have previously been shown to be critical for functioning of a similar enzyme in the protozoan *C. fasciculata*. Mutagenized RihC proteins, purified to greater than 95% purity, showed significant differences in kinetics when assayed by HPLC for uridine and inosine hydrolysis. Changes at four amino acid residues resulted in reductions in velocity when compared to the wild type enzyme for hydrolysis of uridine. These results support the critical roles for these residues for enzyme activity.

## TABLE OF CONTENTS

LIST OF FIGURES .....	vii
LIST OF TABLES .....	viii
LIST OF APPENDICES.....	ix
CHAPTER I: INTRODUCTION.....	1
CHAPTER II: METHODS .....	6
Plasmid Construct.....	6
Site-directed Mutagenesis.....	6
Transformation of BL21 (DE3) pLysS Competent Cells .....	10
DNA Sequencing of Plasmid Inserts .....	10
Restriction Digest of <i>rihC</i> Plasmids .....	14
Agarose Gel Electrophoresis.....	15
Induction of <i>rihC</i> with in BL21 (DE3) pLysS .....	16
Purification of Induced Proteins .....	16
Quantification of Proteins .....	17
Electrophoretic Analysis of Recombinant Proteins .....	18
Western Blot Analysis .....	19
Enzyme Activity Assay.....	20
CHAPTER III: RESULTS.....	22
Comparison of Ribonucleoside Hydrolases.....	22
<i>In vitro</i> Mutagenesis .....	26

Protein Expression and Purification.....	27
High-Performance Liquid Chromatography and Kinetic Analysis .....	27
CHAPTER IV: DISCUSSION .....	31
REFERENCES .....	37

## LIST OF FIGURES

Figure 1. pET-28b- <i>rihC</i> expression vector map .....	7
Figure 2. Multispecies IU-NH clustalW alignments.....	23
Figure 3. ClustalW comparison of <i>C. fasciculata</i> and <i>E. coli</i> nucleoside hydrolases .....	24
Figure 4. Amino acid changes in RihC .....	25
Figure 5. Coomassie blue staining of mutagenized RihC.....	28
Figure 6. Western blot of purified RihC derivatives.....	29

## LIST OF TABLES

Table 1. QuikChange site-directed primer sets.....	8
Table 2. <i>rihC</i> sequencing primers.....	13
Table 3. Hydrolysis velocities of RihC and derivatives of uridine and inosine. ....	30



## LIST OF APPENDICES

APPENDIX A: Buffers and Solutions.....	41
APPENDIX B: Ground State of Uridine .....	45
APPENDIX C: <i>In silico</i> Digestion of RihC.....	46
APPENDIX D: Thrombin Digestion of RihC .....	47
APPENDIX E: RihC Characteristics and Amino Acid Composition.....	48
APPENDIX F: Estimations of RihC Hydrophilicity .....	49
APPENDIX G: Structural Algorithms for RihC .....	50
APPENDIX H: <i>E. coli</i> Purine and Pyrimidine Pathway.....	51
APPENDIX I: Novagen pET-28a-c (+) Vector Technical Bulletin .....	52

## CHAPTER I: INTRODUCTION

Nucleoside hydrolases (NHs) are distributed widely throughout organisms and have been described in bacteria (1, 2), yeast (3), protozoa (4, 5), insects (6), and mesozoa (7). Genes with the characteristics of NHs are found in plants, amphibians and fish but no NHs have been described in mammals (8, 9). The role of NH in prokaryotes and higher eukaryotes has been the subject of debate. Urh1, a uridine-cytosine-specific nucleoside hydrolase of the yeast *Saccharomyces cerevisiae*, has been reported to play a role in pyrimidine salvage (3). More recently, Urh1 has been implicated in a Sir2 regulation as part of the Urh1/Pnp1/Meu1 pathway (10). The accepted function of parasitic protozoan NHs is nitrogenous base salvage. Purine-auxotrophic protozoa depend solely on NHs to scavenge exogenous purines from their hosts because they lack a de novo pathway for purine synthesis (11). However in the bacterium, *Bacillus subtilis*, the NH prevents sporulation by the reduction of inosine, a major trigger of spore germination (12). The various functions of NHs raise questions about their possible roles that are not directly related to nucleotide catabolism.

The dichotomy between mammalian and protozoan purine pathways has provided a target for antibiotics directed at the protozoan NHs (13). The resurgence of malaria in many countries has put 3.2 billion people at risk of malaria with up to 500 million new cases per year resulting in over 1 million deaths per year (14). The malarial surge, with many strains being resistant to monotherapies, reinforces the need for new chemotherapeutics against protozoan parasites. NHs have become important targets of logically designed antiprotozoan drugs to address this need (15, 16).

Nucleoside hydrolases, a superfamily of  $\text{Ca}^{2+}$  dependent metalloenzymes, are glycosidases that hydrolyse the N-glycosidic bond of  $\beta$ -ribonucleosides giving rise to the free nucleic base and ribose (8, 17). The members of this family have shown stringent specificity for the ribose group but are promiscuous when considering the nucleic base. A conserved N-terminal motif, DXDXXXDD, is considered indicative of NH activity (8). Classification of NH on the basis of substrate specificity has given rise to four groups: purine specific (IAG-NH), nonspecific (IU-NH), pyrimidine-specific (CU-NH) and 6-oxopurine-specific (GI-NH). Sequence homology and conservation of active-site residues can also be used to group the NHs (18). The determination of substrate specificity can be inferred from sequences based on either a tryptophan or histidine at a specific active-site residue. Three groups arise from primary sequence data, group I includes nonspecific and pyrimidine specific NHs, group II is comprised of purine-specific NHs (18, 19). Group III proteins are from multicellular organisms and show a cysteine at the conserved histidine binding site which indicates a potentially different catalytic mechanism for the group III proteins (19).

NHs may have a role in the purine salvage pathway in the trypanosome, *Crithidia fasciculata* (11, 20). *C. fasciculata* does not infect mammals but has genetics similar to *Trypanosoma* and *Leishmania* species making it an attractive model organism (21). The most abundant NH of *C. fasciculata* is the group I IU-NH, which has been a model for antiprotozoan drug studies (11). IU-NH of *C. fasciculata* is a nonspecific NH that hydrolyses all commonly occurring purines and pyrimidines but is most efficient at hydrolysing the purine, inosine, and the pyrimidine, uridine (22). This enzyme is a

homotetramer of 34 kDa subunits and has two binding regions: one with affinity to ribose and the other to the leaving group (23). The ribose binding region requires 2'-, 3'-, and 5'-hydroxyls for efficient binding of the ribose moiety (11). The *C. fasciculata* IU-NH residues required for the binding of hydroxyls include Asp-10, Asp-14, Asp-15, Asn-39 and Asp-242 for the 2'- and 3'-hydroxyl and Asn-160, Glu-166, and Asn-168 for the 5'-hydroxyl (24). The NH catalysis of inosine proceeds with an oxocarbenium-like transition state (23). A partial negative charge occurs at the nitrogenous base requiring the protonation of the leaving group for catalysis to proceed. His241 was proposed to provide the necessary protonation for the efficient hydrolysis of inosine by Gopaul *et al.* (22). They showed H241A site-directed mutant had a 2100-fold reduction in activity but maintains comparable activity toward *p*-nitrophenyl  $\beta$ -D-ribofuranoside, which does not require a proton donor (22).

Elemental analysis has shown that  $\text{Ca}^{2+}$  binds at a 1:1 molar ratio with contacts from Asp15, Asp242, and Asp10, and the main-chain carbonyl of Thr126 with one ordered water at the bottom of a deep cavity (25). The reaction is not inhibited when assayed with 10 mM EGTA in the reaction mixture but extended incubation with EGTA does cause loss of activity, which can be restored by addition of  $\text{Ca}^{2+}$  to the reaction mixture. This indicates the  $\text{Ca}^{2+}$  is tightly bound by the enzyme and necessary for reaction (25). Activation of IU-NH's water nucleophile could occur by  $\text{Ca}^{2+}$ - $\text{H}_2\text{O}$  interaction, acting to decrease the  $\text{pK}_a$  for the bound water with subsequent proton transfer to carboxyl oxygen of Asp10 as the incipient hydroxyl ion attacks, following formation of the ribosyl-oxocarbenium ion, as is supported by observations of Asp10Ala mutants

(25). This information points to the role of the  $\text{Ca}^{2+}$  to orient the substrate in the active site and to position the water molecule for attack at the C1'-anomeric carbon following the formation of the ribooxocarbenium ion (24).

The transition state of *C. fasciculata* IU-NH has been studied using multiple kinetic isotope effects (KIE) and bond-energy bond-order vibrational analysis (BEBOVIB) (23). The isotope effects indicate that the enzyme stabilizes an  $\text{S}_{\text{N}}1$ -like transition state with substantial oxocarbenium ion character. The transition state also has a protonated leaving group, a glycosidic linkage that is almost cleaved, and an enzyme-directed attacking O nucleophile with low bond order to the target carbon(23). Understanding the transition state of NHs provides a better understanding of the interaction between the enzyme and its substrates.

RihC is a nonspecific NH that hydrolyzes common nucleosides. This bacterial enzyme is similar to the IU-NH of *C. fasciculata* and shares amino acids at the active site that are critical for interacting with substrates. RihC also exhibits a similar transition state to the *C. fasciculata* enzyme including the formation of an oxocarbenium ion, either protonation of or the formation of a hydrogen bond to O2 to activate the heterocyclic base, a broken C-N glycosidic bond, and incomplete bond formation with the attacking nucleophile (26).

The current study examines the amino acid residues that may be critical in catalyzing the hydrolysis of nucleosides by *E. coli* RihC. Site-directed mutagenesis was used to introduce mutations leading to changes in amino acid residues shown to be critical for *C. fasciculata* IU-NH. The goal of this study was to measure changes in

enzyme activity in response to the introduction of the mutations in order to confirm the critical role of these amino acids for the activity of *E. coli* RihC.

## CHAPTER II: METHODS

### Plasmid Construct

The pET28-*rihC* plasmid was graciously provided by Dr. Massimo Degano of the San Raffaele Scientific Institute, Milan, Italy. Within the multi-cloning site of the plasmid, the 912 bp *rihC* gene and its own stop codon (NCBI GenBank accession number U00096) was cloned between *Nde* I and *Xho* I of the approximately 5300 bp pET28b vector (Novagen/EMD Millipore, Billerica, MA; Fig. 1). The pET vector contains a kanamycin resistance cassette for selection with in BL21(DE3) pLysS *E. coli* (Stratagene®, La Jolla, Ca) and a pBR322 origin. The gene was fused with a vector-encoded N-terminal hexahistidine tag. The expression is under the control of the T7 RNA polymerase with a T7 promoter and is located upstream of the *Nde* I site between positions 370 and 386. The plasmid was subjected to restriction digest and DNA sequencing to confirm the accuracy of the insert location.

### Site-directed Mutagenesis

The Stratagene® QuickChange® Site-directed Mutagenesis kit (Stratagene®, La Jolla, Ca) was used to change amino acid residues at positions 14, 15, 164, 222, 233, 234, 241, and 242 to alanine. Primers (Integrated DNA Technologies, Inc., Coralville, IA) were designed to the *E. coli* K12 *rihC* nucleotide sequence (NCBI GenBank accession number U00096) using the QuickChange® primer design program (<http://www.stratagene.com/sdmdesigner/default.aspx>) and are listed in Table 1.

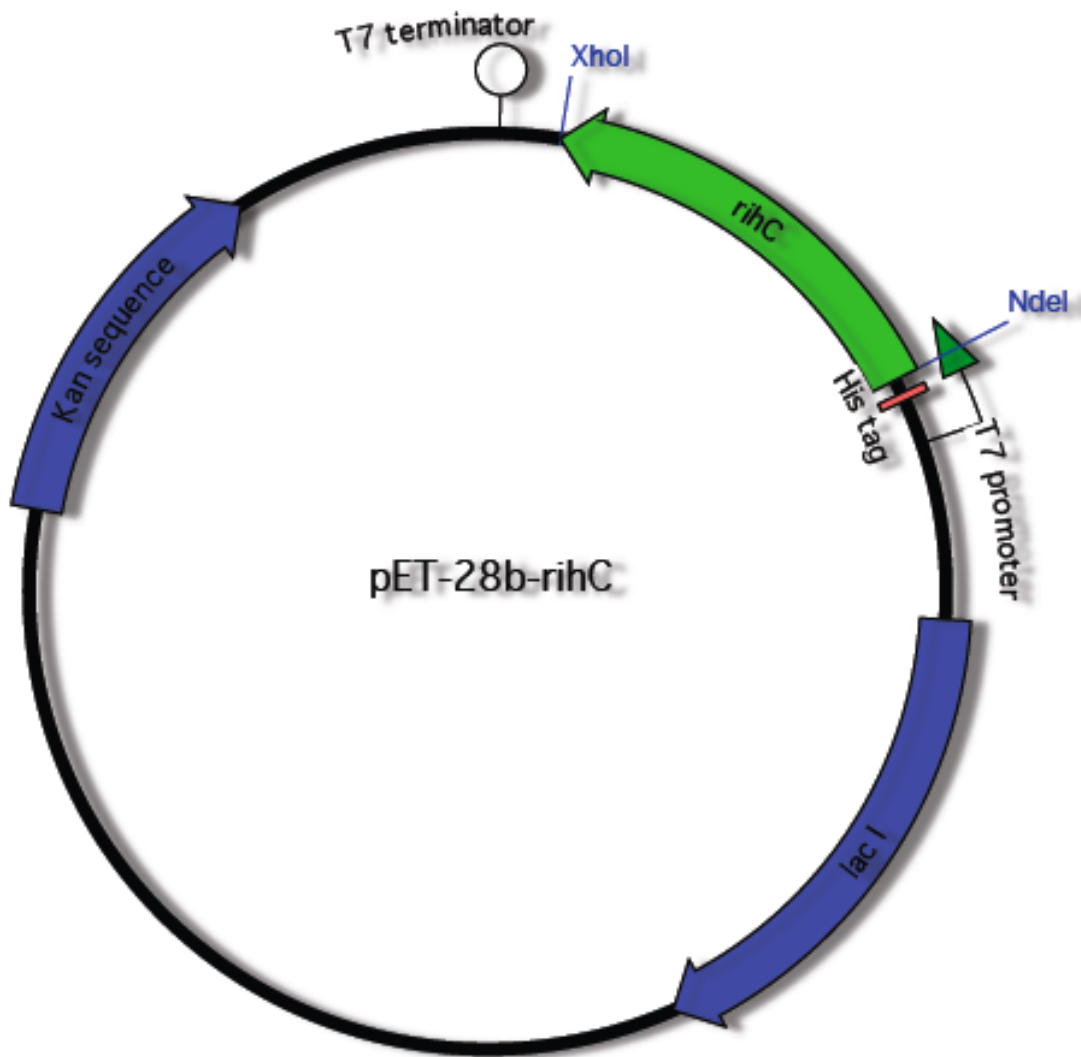


**Figure 1. pET-28b-rihC expression vector map.** The expression plasmid construction is shown. The gene encoding *rihC* was directionally cloned between *Nde* I and *Xho* I restriction sites in frame with a plasmid-encoded histidine tag to produce a fusion protein when translated.



**Table 1. QuikChange site-directed primer sets.**

Name	Sequence	DNA Bases	%GC	Tm
D14A	5'-ACC CCG GCA TTG CCG ATG CCG TCG C-3'	25	72.0	80.0
D14Aanti	3'-TGG GGC CGT AAC GGC TAC GGC AGC G-5'	25	72.0	80.0
D15A	5'-CCC GGC ATT GAC GCT GCC GTC GCC ATT-3'	27	67.0	80.1
D15Aanti	3'-GGG CCG TAA CTG CGA CGG CAG CGG TAA-5'	27	67.0	80.1
F164A	5'-TGT ACG CCA AAC GCC GAG GCT AAT ATT GCT GCC GAT CC-3'	38	55.2	81.1
F164Aanti	3'-ACA TGC GGT TTG CGG CTC CGA TTA TAA CGA CGG CTA GG-5'	38	55.2	81.1
R222A	5'-CCC TGT TTA GCC ACT ACG CTA GCG GCA GTA TGC AAA-3'	36	52.7	78.8
R222Aanti	3'-GGG ACA AAT CGG TGA TGC GAT CGC CGT CAT ACG TTT-5'	36	52.7	78.8
H233A	5'-GCG GCT TGC GAA TGG CCG ATC TCT GCG CCA-3'	30	66.6	79.7
H233Aanti	3'-CGC CGA ACG CTT ACC GGC TAG AGA CGC GGT-5'	30	66.6	79.7
D234A	5'-CTT GCG AAT GCA CGC TCT CTG CGC CAT CG-3'	29	62.0	80.2
D234Aanti	3'-GAA CGC TTA CGT GCG AGA GAC GCG GTA GC-5'	29	62.0	80.2
L241A	5'-GCC ATC GCC TGG GCG GTG CGC CCG GA-3'	26	80.7	81.0
L241Aanti	3'-CGG TAG CGG ACC CGC CAC GCG GGC CT-5'	26	80.7	81.0
V242A	5'-CGC CTG GCT GGC GCG CCC GGA CC- 3'	23	87.0	83.5
V242Aanti	3'-GCG GAC CGA CCG CGC GGG CCT GG- 5'	23	87.0	83.5

The melting temperature ( $T_m$ ) of these primers was calculated using the formula  $T_m = 81.5 + 0.41(\% \text{ GC}) - 675/N - \% \text{ mismatch}$ , where  $N$  is the primer length in bases, and  $\% \text{ GC}$  and  $\% \text{ mismatch}$  are integers. The primers met the suggested specifications of having a  $T_m$  of greater than  $78^\circ\text{C}$  and greater than 40% GC content as specified by the manufacturer of the QuickChange® kit. A concentration of 125 ng of each primer was used in the mutagenesis protocol.

The 50  $\mu\text{L}$  QuickChange® reaction mixture included 5  $\mu\text{L}$  of 10X QuickChange® reaction buffer, 1  $\mu\text{L}$  of dNTP mix (Stratagene), 50 ng of pET28-*rihC* plasmid from *dam*<sup>+</sup> BL21 (DE3) pLysS *E. coli*, and 125 ng of corresponding forward and reverse primers. The total volume was adjusted to 50  $\mu\text{L}$  with ddH<sub>2</sub>O, and then 1  $\mu\text{L}$  of PfuTurbo® DNA polymerase (2.5 U/ $\mu\text{L}$ ; Stratagene) was added to the reaction mixture. The reaction mixture was amplified in an MJ Research PTC-200 (PTC200) DNA Engine thermal cycler (Bio-Rad, Hercules, CA). PCR amplification cycles included a  $95^\circ\text{C}$  denaturation step for 5 min. This step was followed by 16 cycles of melting at  $95^\circ\text{C}$  for 30 sec, annealing at  $55^\circ\text{C}$  for 1 min, elongation at  $68^\circ\text{C}$  for 6 min, and a final  $4^\circ\text{C}$  incubation to lower reaction mixture temperature to less than  $37^\circ\text{C}$ .

Following PCR, 1  $\mu\text{L}$  of *Dpn* I (10 U/ $\mu\text{L}$ ) (Stratagene) was added to each amplification reaction and mixed by centrifugation. The mixture was incubated at  $37^\circ\text{C}$  for 1 h and the digested mixture was used to transform competent *E. coli* BL21 (DE3) pLysS cells.

### **Transformation of BL21 (DE3) pLysS Competent Cells**

A 100  $\mu$ L aliquot of BL21 (DE3) pLysS competent *E.coli* cells (Stratagene) were thawed on ice then transferred to pre-chilled 50-mL BD Falcon polypropylene tubes (BD Biosciences, Franklin Lakes, NJ). Fresh  $\beta$ -mercaptoethanol (Stratagene) was added to a final concentration of 25 mM and the mixture was incubated for 10 min, swirling gently every 2 min. A negative control reaction was performed using 1  $\mu$ L of sterile ultrapure water. A 1  $\mu$ L aliquot of pUC18 was used for a positive control reaction. The experimental transformations were performed with a plasmid DNA concentration of 0.5 ng/ $\mu$ L. After addition of DNA, the reactions were incubated on ice for 30 min followed by a 45 sec 42°C heat-pulse. The cells were then incubated on ice for 2 min. After incubation, 0.9 mL of preheated (42°C) SOC medium was added to the cells and incubated at 37°C with shaking at 225 rpm for 1 h. Following this incubation, 100  $\mu$ L of cells were spread onto LB agar plates containing 34  $\mu$ g/mL chloramphenicol (Sigma-Aldrich, St. Louis, MO) and 50  $\mu$ g/mL kanamycin (Sigma-Aldrich), and incubated overnight at 37°C.

Multiple transformant colonies were chosen and were later analyzed by PCR, restriction digest, protein expression, and DNA sequencing to determine the most fit transformant for later studies.

### **DNA Sequencing of Plasmid Inserts**

DNA sequencing was performed on sense and antisense strands to determine the accuracy of the *rihC* gene when compared to the NCBI published sequence and to confirm the desired mutations were present following the mutagenesis (GenHunter

Sequencing, Nashville, TN). T7term and NcoF sequencing primers directed to plasmid sequences and *rihC* gene-specific sequence primers C357 and 421R were designed using the published sequences from Novagen (Appendix I) and the NCBI database (NCBI GenBank accession number U00096).

The DNA template was purified by following the protocol for the QIAprep® Spin Miniprep kit (Qiagen Inc., Valencia, CA). Briefly, cells from a 5 mL overnight culture of BL21 (DE3) pLysS *E. coli* cells containing the pET28b-*rihC* plasmid or pET28b plasmids with the putative mutation were pelleted at 7,000 rpm for 10 min and then completely resuspended in 250 µL of P1 buffer. A 250 µL volume of P2 buffer was then added and mixed by gently inverting 6 times followed by incubation for 5 min at room temperature. The neutralizing buffer, N3, was added and immediately mixed by inverting gently 6 times causing the mixture to become cloudy. The mixture was centrifuged for 10 min at 13,000 rpm in an Eppendorf 5415D microcentrifuge (Hauppauge, NY). The supernatant was transferred to the Qiaprep spin column by pipette and then centrifuged for 1 min at 13,000 rpm. The flowthrough was discarded and then 0.5 mL of PB buffer was added to the spin column. The column was again centrifuged at 13,000 rpm for 1 min and flow through was discarded. A 0.75 mL volume of PE buffer was added to column and centrifuged for 1 min at 13,000 rpm and the flowthrough was again discarded. The spin column was then placed into a DyNA Vap centrifugal evaporator for 3 min to remove residual ethanol form PE buffer. The spin column was inserted into a clean microcentrifuge tube and 30 µL of ddH<sub>2</sub>O was added to the center of the spin column membrane and allowed to stand for 1 min. The column was

then centrifuged for 1 min at 13,000 rpm and the flowthrough was collected as the plasmid DNA. The concentration of this purified plasmid DNA was then quantified with an Amersham GeneQuant spectrophotometer (GE Healthcare, Piscataway, NJ) by measuring the absorbance at 260 nm.

The DNA sequencing reactions used puRe Taq Ready-To-Go PCR Beads (GE Healthcare). These beads, when reconstituted to 25  $\mu$ L, contain 2.5 units of puRe Taq DNA polymerase, 200  $\mu$ M of dATP, dCTP, dGTP, and dTTP in 10mM Tris-HCl (pH 9.0 and room temperature), 50 mM KCl and 1.5 mM MgCl<sub>2</sub>. Each reaction mixture included 1 ng of template plasmid DNA, 25 pmol of sequence primer (Table 2), and the appropriate volume of nuclease free water (Applied Biosystems/Ambion, Austin, TX) for a total volume of 25  $\mu$ L. The reaction mixtures were prepared within a laminar flow hood and amplified in an MJ Research PTC-200 DNA Engine thermal cycler. The reactions were subjected to a 5 min 94°C denaturation step followed by 35 cycles of denaturation at 94°C for 30 sec, annealing at 56°C for 30 sec, and extension at 72°C for 1 min. Once the protocol was complete, the products were held at 4°C or stored at -20°C.

Before sequencing, the sequencing reactions were purified using the QIAquick PCR Purification Kit (Qiagen). A 125  $\mu$ L volume of PB buffer (5 volumes) was added to the PCR sample. The sample was added to the Qiaquick column and centrifuged at 13,000 rpm for 1 min. The sample was then washed with 0.75 mL of PE buffer, centrifuged for 1 min at 13,000 rpm, and the flowthrough was discarded. The spin column was then placed into a DyNA Vap centrifugal evaporator for 3 min to remove

**Table 2. *rihC* sequencing primers.**

Name	Sequence	DNA Bases	%GC	Tm
NcoF	5'-TAT ACC ATG GGC AGG AGC-3'	18	55.6	55.5
C357	5'-CCG TTA ACC AAT ATT GCG CT-3'	20	45.0	60.0
T7term	5'-GCT AGT TAT TGC TCA GCG G-3'	19	52.6	53.4
421R	5'-AAT ATA CGG CTT GCA TTC CG-3'	20	45.0	60.0

residual ethanol from the PE buffer. The Qiaquick column was then placed in a microcentrifuge tube and the DNA was eluted with 30  $\mu$ L of nuclease free water (Applied Biosystems/Ambion). The DNA concentration of the elution was determined absorbance at 260 nm on a spectrophotometer, followed by sequencing by GenHunter (Nashville, TN). The sequences were assembled using MacVector 10.5 with assembler. The assembled sequences were translated *in silico* and aligned against the published sequence.

### **Restriction Digest of *rihC* Plasmids**

The location of the *rihC* insert was verified by a double digest with *Nco* I and *Xho* I (New England Biolabs, Beverly, MA). A reaction was prepared on ice to digest 50 ng of pET28b-*rihC*. The digest mixture contained 5  $\mu$ L of NEB 10X buffer 2 (New England Biolabs; 1X buffer 2 contained 50 mM NaCl, 10 mM Tris-HCl, 10 mM MgCl<sub>2</sub>, 1 mM dithiothreitol (DTT) with a pH of 7.9 at 25°C). The digest mixture also contained 0.5  $\mu$ L of 100X bovine serum albumin (BSA), 0.2 U/ $\mu$ L each of restriction enzymes *Nco* I and *Xho* I, and nuclease free H<sub>2</sub>O (Applied Biosystems/Ambion) for a total volume of 50  $\mu$ L.

The mixture was placed in an MJ Research PTC-200 DNA Engine thermal cycler, programmed to maintain the mixture at 37°C for 1 h. After 1 h, enzymes were heat inactivated for 20-min at 65°C and then held at 4°C or stored at -20°C.

A gene-specific single digest was also performed. The *rihC* sequence (NCBI GenBank accession number U00096) was digested *in silico* using NEBcutter V2.0 (New England Biolabs) to generate a list of enzymes that produce single cuts in the gene. The

list of single cutters was crossed referenced with the published restriction sites of the pET28 plasmid (Appendix I). The enzyme *Bsu36 I* was used to set up the gene specific digest (Promega, Madison, WI). The digest was prepared on ice to digest 1  $\mu\text{g}$  of pET28b-*rihC*. The mixture contained 2  $\mu\text{L}$  of 10X buffer E, which at 1X is composed of 6 mM Tris-HCl (pH 7.5), 100 mM NaCl, 6 mM  $\text{MgCl}_2$ , and 1 mM DTT. In addition, acetylated BSA was added to a final concentration of 0.1  $\mu\text{g}/\mu\text{L}$  and *Bsu36 I* at a final concentration of 0.25 U/ $\mu\text{L}$ . Nuclease free water (Applied Biosystems/Ambion) was added for a total volume of 20  $\mu\text{L}$ .

The digestion mixture was incubated at 37°C using a MJ Research PTC-200 DNA Engine thermal cycler for 1 h and held at 4°C or stored at -20°C. The single and double digests were then analyzed by agarose gel electrophoresis.

### **Agarose Gel Electrophoresis**

All PCR products and restriction enzyme digests were analyzed by agarose gel electrophoresis to ensure the proper sized pieces of DNA. TAE running buffer (1X) was prepared with 40 mM Tris acetate (pH 8.3) and 1 mM EDTA. A 0.50 g amount of agarose (Sigma-Aldrich, Saint Louis, MO) was added to 50 mL of previously made running buffer and microwaved to produce a 1% (w/v) agarose gel solution. After the agarose was dissolved, ethidium bromide was added to a final concentration of 7  $\mu\text{g}/\text{mL}$ . The gel was submerged in the Bio-Rad mini-sub cell GT apparatus powered by the Bio-Rad PowerPac Basic™. A 7  $\mu\text{L}$  volume of Sigma-Aldrich PCR Marker (Product No. P 9577) was loaded into the gel, and 2  $\mu\text{L}$  of Sigma-Aldrich 6X PCR loading buffer (Product No. P 7206) was added to 10  $\mu\text{L}$  of each sample. The DNA was separated at



120 V for 10 min followed by 30 min at 100 V. The gels were viewed and documented using the Bio-Rad Universal Hood imaging system.

### **Induction of *rihC* with in BL21 (DE3) pLysS**

A 25 mL overnight culture of transformed *E. coli* in LB broth containing kanamycin (50 µg/ml) and chloramphenicol (50 µg/ml) was used to inoculate 500 mL of LB containing no antibiotics. The 500 mL culture was incubated at 37°C with shaking at 220 rpm for 2 h. A 100 µL aliquot was removed as an “un-induced sample” and stored on ice for later analysis. The induction culture was grown to an optical density at 600 nm (OD<sub>600</sub>) of 0.600 by incubation at 37°C and shaking at 220 rpm. A final concentration of 1 µM isopropyl-1-thio-β-D-galactopyranoside (IPTG) was added to the culture and incubation was continued for 3 h leading to over-expression of *rihC*. A 100 µL sample was removed for analysis as the “induced non-purified sample.” The remainder of the induced sample was then processed for purification.

### **Purification of Induced Proteins**

Previously induced 500 mL cultures were centrifuged at 4°C and 10,000 rpm for 15 min in a Sorvall SS-34 rotor in a Sorvall RC6 centrifuge (Thermo Fisher Scientific, Pittsburgh, PA). The cells were washed twice in 3 mL of wash/equilibration buffer by centrifuging at 4°C and 7,000 rpm for 15 min. The washed cells were then suspended in wash/equilibration buffer (50 mM sodium phosphate, pH 8.0, 0.3 M sodium chloride and 10 mM imidazole) and sonicated on ice for 15 sec burst at 60% amplitude followed by a 2-min incubation on ice for a total of 4 cycles. The cell debris was removed by centrifugation to produce a cleared lysate.

The cleared lysate was loaded onto a prepared His-Select column and allowed to flow through at a rate not greater than 1 mL/min. The column was then washed with wash/equilibration buffer until the absorbance at 280 nm was 0. The purified protein was eluted using elution buffer (same as wash/equilibration buffer with 250 mM imidazole) such that a 50 mL volume of elution buffer was collected. The collected elution was added to YM10 Centricon centrifugal concentrator (EMDMillipore) with a MW cutoff of 10 kD and concentrated 25-fold to a 2 mL volume. The concentrated elution was then dialyzed for 48 h against 1 L of 10 mM Tris and 0.5 mM DTT (pH 7.2) at 4°C. The Tris-DTT solution was exchanged after 24 h. The sample was quantified and analyzed with SDS-PAGE.

### **Quantification of Proteins**

The quantification of overexpressed protein was performed by two methods. After purification and dialyzation, both an absorbance at 280 nm and Bio-Rad Protein Assay were used to determine the amount of protein for all samples. Spectrophotometric measurements at an of absorbance of 280 nm were taken for each sample using the GeneQuant Pro spectrophotometer with 10 mM Tris (pH 7.2) and 0.5 mM DTT as the blank. An absorbance at 260 nm was also recorded for each sample. The entire volume of sample was transferred to a clean cuvette without dilution. The readings were then converted to molar concentration of protein (c) using the Beer-Lambert Law as follows:  $A = \epsilon cl$ , where A is absorbance at 280 nm, the molar absorption coefficient,  $\epsilon$ , equals 22960, and l is 1-cm pathlength.

The Bio-Rad Protein Assay was also used in a microscale format to determine the quantity of protein. A 96-well plate was used to set-up all samples, blank, and standards

in triplicate. A 100  $\mu\text{g}/\text{mL}$  BSA working stock was made from 2  $\text{mg}/\text{mL}$  BSA and used to produce a standard dilution curve. The standard curve used contained 100, 80, 60, 40, 20, 10, and 5  $\mu\text{g}/\text{mL}$  concentrations of BSA. Volumes of 160  $\mu\text{L}$  of each standard, blank, and sample were placed into wells of the 96-well plate in triplicate, and then 40  $\mu\text{L}$  of Bio-Rad dye reagent and mixed into each well by pipetting. The plate was incubated at room temperature and was mixed for 30 sec every 3 min for 15 min within a VersaMax microplate reader with SoftMax® Pro software suite. The plate was mixed continuously for 1 min immediately prior to reading the absorbance at 595 nm with a blank of 10 mM Tris (pH 7.2) and 0.5 mM DTT. SoftMax® Pro software was used to interpolate the concentration from the standard curve.

### **Electrophoretic Analysis of Recombinant Proteins**

Sodium dodecyl sulfate polyacrylamide gel electrophoresis (SDS-PAGE) was used to analyze the expression and purity of the recombinant proteins. The soluble fraction of induced cell lysates of punitive mutants and concentrated dialyzed eluant proteins were analyzed in this fashion. To prepare samples for the gel, 50  $\mu\text{L}$  of  $\beta$ -mercaptoethanol (Sigma-Aldrich) was added to 950  $\mu\text{L}$  of Laemmli sample buffer (Bio-Rad). The prepared sample buffer was added to 10  $\mu\text{L}$  of sample at a 1:1 ratio and incubated at 95°C for 5 min. These samples were added to a PAGER® precast gel (Lonza Rockland Inc., Rockland, ME), which had been pre-run for 15 min with 1:10 dilution of premixed 10X Tris-Glycine-SDS (Bio-Rad) in an SE 260 Mighty Small apparatus (Hoefer, Holliston, MA) at 30 mA powered by a 3000xi Electrophoresis Power Supply

(Bio-Rad). Precision Plus Protein standards were loaded alongside samples to provide a comparative measure of protein size. The samples were run at 30 mA constant current.

The gels were then stained with GelCode® Blue Stain Reagent (Pierce Chemical Company, Rockford, IL). First, gels were washed with agitation for 15 min in ultrapure water and then stained with GelCode® Blue Stain Reagent for 1 h. Lastly, the gel was destained by incubating for 1 h with agitation in ultrapure water and imaged as above.

### **Western Blot Analysis**

WesternBreeze® (Invitrogen/Life Technologies, Carlsbad, CA) was used to assess the production of the recombinant protein. Two gels were run using the SDS-PAGE protocol described above with Precision Plus Protein Kaleidoscope standards (Bio-Rad). One gel was stained using GelCode® Blue Stain Reagent. The other gel was used for Western blot analysis. For the Western blot, a transfer of proteins from the gel to a membrane was performed using an Invitrogen (Life Technologies) XCell II™ Blot Module in the XCell II™ Mini-Cell (LifeTechnologies). The apparatus was filled with transfer buffer composed of 25 mM Tris (pH 8.3), 192 mM glycine, and 20% (v/v) methanol. Invitrolon™ PVDF (Invitrogen/LifeTechnologies) was pre-wetted in methanol for 30 sec, rinsed in ultrapure water, and then equilibrated in transfer buffer for 10 min.

The wells (top) and foot (bottom) of the gel to be transferred were removed and the remaining gel was placed onto filter paper wetted with transfer buffer. The filter paper was placed on two blotting pads within the cathode core of the blot module. The equilibrated PVDF was placed directly upon the gel and wetted filter paper was placed over the PVDF membrane. Wet blotting pads were used to fill the remaining space to the

anode of the module. The transfer was then performed at 100 V for 1 h, powered by the Bio-Rad PowerPac Basic™. After the transfer was completed, the membrane was incubated in blocking solution prepared by combining 2 mL of WesternBreeze® Blocking/Diluent part A (Invitrogen/Life Technologies), 3 mL of WesternBreeze® Blocking/Diluent part B, and 5 mL of ultrapure water for 1 h at room temperature. Following blocking, the membranes were rinsed with ultrapure water exchanging water every 5 min up to 20 min.

The membrane was then incubated with a 1:2000 dilution of Anti-HisG-AP AP-conjugated primary antibody (Invitrogen/Life Technologies) in 10 mL of primary antibody diluent, 2 mL WesternBreeze® Blocking/Diluent part A, 1 mL WesternBreeze® Blocking/Diluent part B, and 7 mL ultrapure water. The blot was incubated at 4°C for 2 h with gentle agitation. The blot was washed with 20 mL of 1X WesternBreeze® Antibody Wash for 20 min, exchanging the solution every 5 min. This was followed by a 20-min wash with ultrapure water. The membrane was then incubated with 10 mL of WesternBreeze® Chromogenic Substrate (Invitrogen/Life Technologies) and incubated at 4°C for 24 h. The membrane was rinsed twice with 20 mL of ultrapure water for 2 min each wash. The membrane was dried and imaged as for the SDS-PAGE.

### **Enzyme Activity Assay**

Nucleoside hydrolase activity was determined by HPLC. Reaction mixtures consisted of uridine or inosine at the appropriate concentration in 50 mM Tris (pH 7.2). The total volume of the reaction mixture was 1 mL. The reaction was initiated by the

addition of enzyme (2.0  $\mu\text{g}$ ). At appropriate times, 20  $\mu\text{L}$  aliquots were withdrawn and analyzed by HPLC.

The relative amounts of hypoxanthine and inosine, or uracil and uridine were determined on a ChromTech HPLC system. The system consisted of an ISO-2000 isocratic pump, Rheodyne 7725 injection valve, Model 500 UV/Vis variable wavelength detector, and a PeakSimple Chromatography system. Separation of the nucleosides and bases was achieved on a Phenomenex Phenosphere ODS reverse phase column (150 x 4.6 mm). The mobile phase was 95% (w/v) 10 mM ammonium acetate (pH 5.2) and 5% (v/v) methanol with a flow rate of 1.0 mL/min. Each sample injection was 20  $\mu\text{L}$ . Nucleosides and their corresponding bases were detected at 254 nm. The resulting areas were corrected for the differences in extinction coefficients between the nucleosides and bases. All samples were analyzed in triplicate.

## CHAPTER III: RESULTS

### Comparison of Ribonucleoside Hydrolases

Multiple and pairwise alignments were performed to compare between Inosine-Uridine Nucleoside Hydrolase (IU-NH), the archetype nucleoside hydrolase of *Crithidia fasciculata*, and hydrolases from *Leishmania donovani*, *Anopheles gambiae* str. Pest, *Escherichia coli* and *Bacillus anthracis* (Fig. 2). *C. fasciculata* and *L. donovani* were most similar (90.8% similarity, 80.0% identical). *E. coli* RihC was more similar to eukaryotic nucleoside hydrolases than the Gram-positive *B. anthracis*. RihC was 50.5% similar with 35.6 % of amino acids being identical to *C. fasciculata* IU-NH and had 52.7% similarity with 35.9% amino acid identity when aligned to *L. donovani*, while *B. anthracis* was only 40.9% similar with only 23.6% identical amino acid residues to *E. coli* RihC. There are 37 conserved identities among these 5 proteins.

Alignments comparing IU-NH and the ribonucleoside hydrolases of *E. coli*, RihA, RihB, and RihC, determined that there are 69 conserved amino acid identities. RihC was more similar to RihA (59.8% similar, 43.7% identical) than RihB (54.8% similar, 36.6% identical). The conserved residues of these proteins are depicted in Fig. 3.

RihC residues conserved with IU-NH were identified. Fig. 4 shows the residues of interest. Aspartic acid (D) residues 14, 15, and 234, arginine residues (R) 222 and 233, phenylalanine (F) residue 164, leucine residue (L) 241, and valine residue (V) 242 were changed to alanine (A). Residues 14, 15, 164, 222, 233 and 234 are the interest for this study, while residues 241 and 242 were investigated previously.

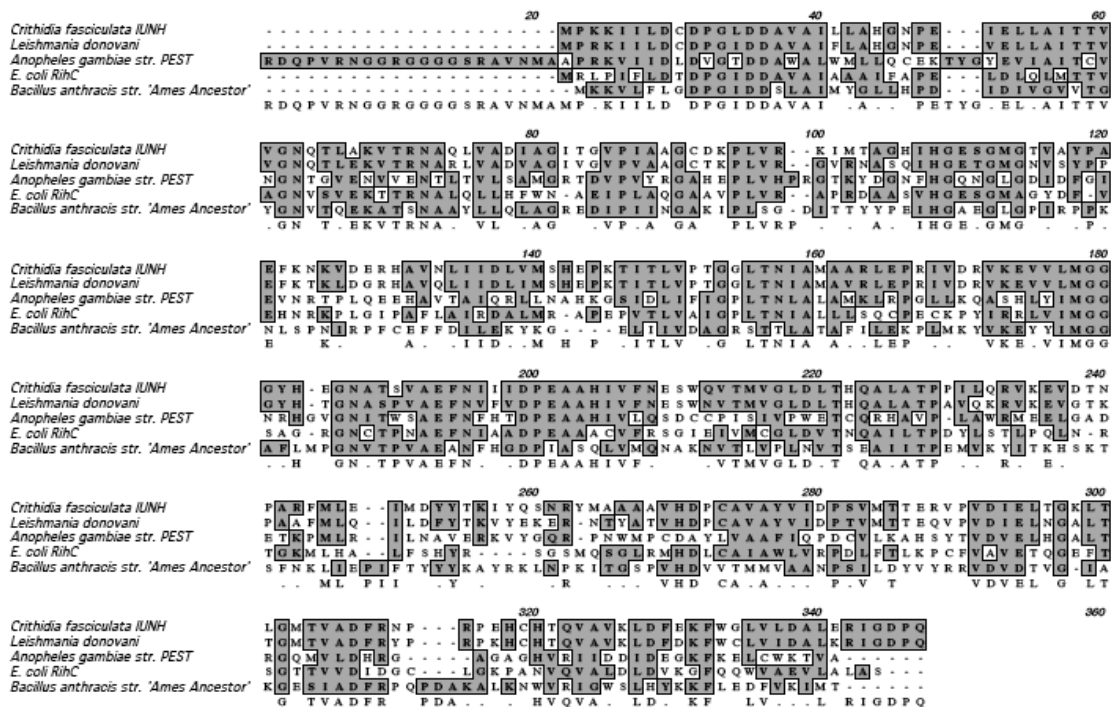
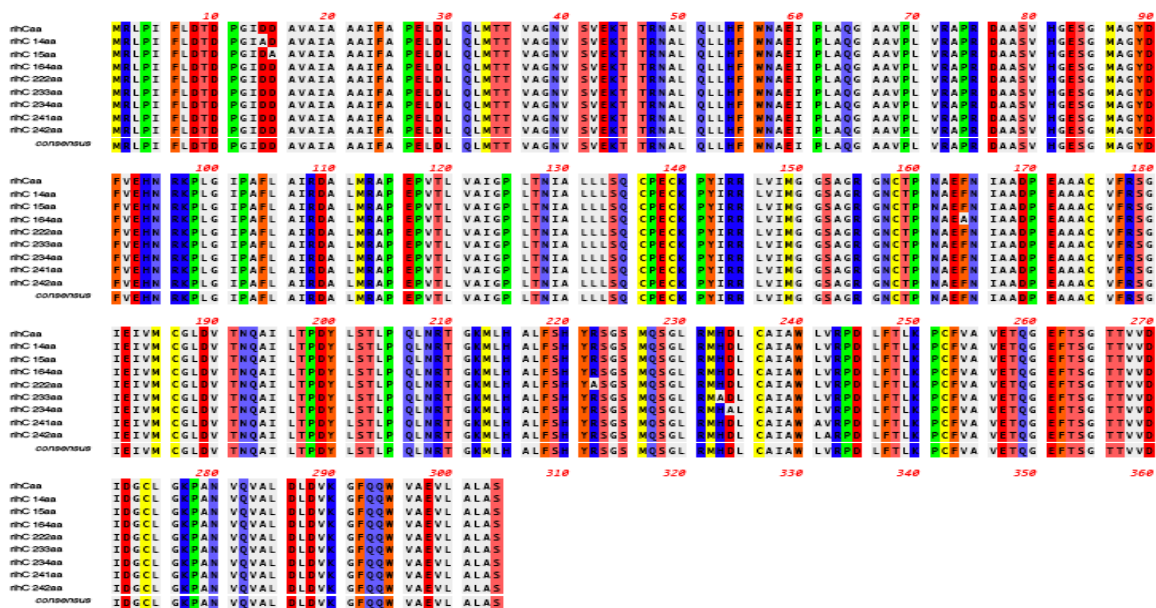


**Figure 2. Multispecies IU-NH clustalW alignments.** Alignments of the archetype IU-NH from *C. fasciculata* as well as homologous proteins from *L. donovani*, *A. gambiae* str. PEST, *E. coli*, and *B. anthracis* are shown. Common residues are noted in grey and the consensus sequence is shown on the last line







### ***In vitro* Mutagenesis**

After receipt of pET28-*rihC* from Dr. Degano, the plasmid was transformed and harbored in BL21 (DE3) pLysS competent *E. coli* cells. Transformants were selected on LB agar containing 34 µg/mL chloramphenicol (cam<sup>R</sup>) to maintain pLysS and 50 µg/mL kanamycin (kan<sup>R</sup>). Colonies with the correct resistance profile, cam<sup>R</sup> and kan<sup>R</sup>, were selected for analysis to determine the suitability for downstream mutation of the plasmid being harbored. Plasmids were then purified by Qiagen mini-prep, and those with a ratio of the absorbance at 260 and 280 nm greater than 1.80 were subjected to restriction enzyme digestion with *Xho* I and *Nde* I and visualized by agarose gel, resulting in two bands of approximately 1000 bp (*rihC*) and 5300 bp (plasmid). Plasmids with the appropriate restriction profile were subjected to Sanger DNA sequencing using appropriate primers (Table 2). These data allowed confirmation that the plasmid pET28a-*rihC* encodes an RihC-hexahistidine fusion protein (Fig. 1).

Following confirmation of the parental plasmid, site-directed mutants were generated to mutate specific amino acid residues hypothesized to be critical for enzyme function. The Quickchange™ protocol was employed and the primers listed in Table 1 were used to introduce mutations to the nucleic acid sequence of the gene. The resultant plasmids were obtained by Qiagen mini-prep and sequenced by Sanger DNA sequencing. The sequences were assembled, translated, and amino acid sequences aligned *in silico* using MacVector with assembler. The resulting sequences have the desired changes in amino acid sequence (Fig. 4).

## **Protein Expression and Purification**

Overexpressions of wild-type and mutant derivatives were performed by induction with 10 mM IPTG in LB with antibiotic pressure. After lysis of induced cells by sonication, the soluble fraction was applied to an Ni agarose affinity chromatography column. RihC was determined to be > 95% pure as estimated by densitometry (Kodak 1D software) of electrophoretically separated proteins (Fig. 5). The presence of a histidine-tag for all recombinant proteins was confirmed by Western blotting with anti-his antibody (Fig. 6).

## **High-Performance Liquid Chromatography and Kinetic Analysis**

The hydrolysis of uridine and inosine was assayed via HPLC. Time-course analysis was performed and resulting areas under the curve (AUC) for chromatograms were collected and analyzed to determine velocities. These data show that RihC nucleoside turnover is 12.9 and 8.72  $\mu\text{mol}/\text{min}/\text{mg}$  for uridine and inosine, respectively. Changes at residues 14, 164, and 234 resulted in the approximately 50-fold reductions when compared to the wild type enzyme for hydrolysis of uridine. Mutation D15A resulted in 100-fold reduction, exhibiting the least activity of any of the tested proteins. The remaining mutants had fold changes less than 5-fold and are likely not significant with regard to uridine hydrolysis. Although mutation H233A did not have a great effect on activity toward uridine (3.6-fold reduction), the mutation reduced the velocity by greater than 58-fold to 0.15  $\mu\text{mol}/\text{min}/\text{mg}$  for inosine (Table 3).

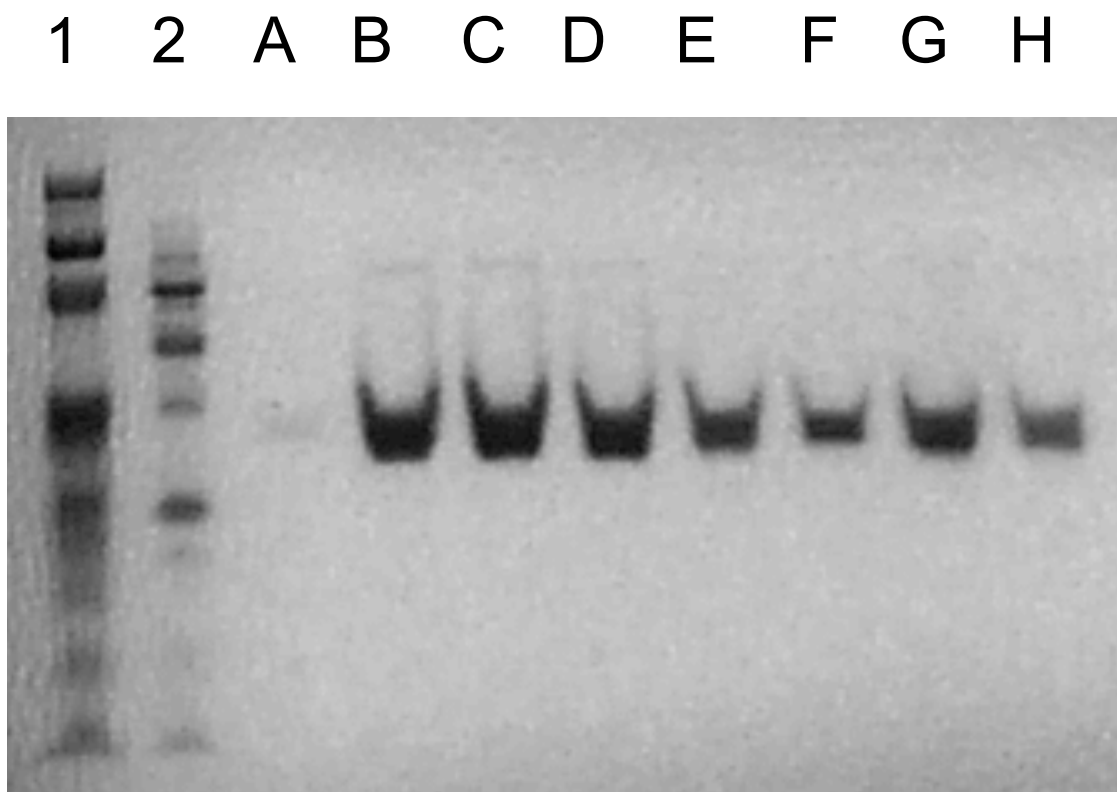


**Figure 5. Coomassie blue staining of mutagenized RihC.** Purified RihC derivatives were size-fractionated by SDS-PAGE. The lanes were loaded as follows: 1) Kaladiscope standard, 2) unstained standard, A) D14A, B) D15A, C) F164A, D) R222A, E) H233A, F) D234A, G) L241A, and H) V242A. The gel shows a single band of the same size (34 kDA) for all samples.

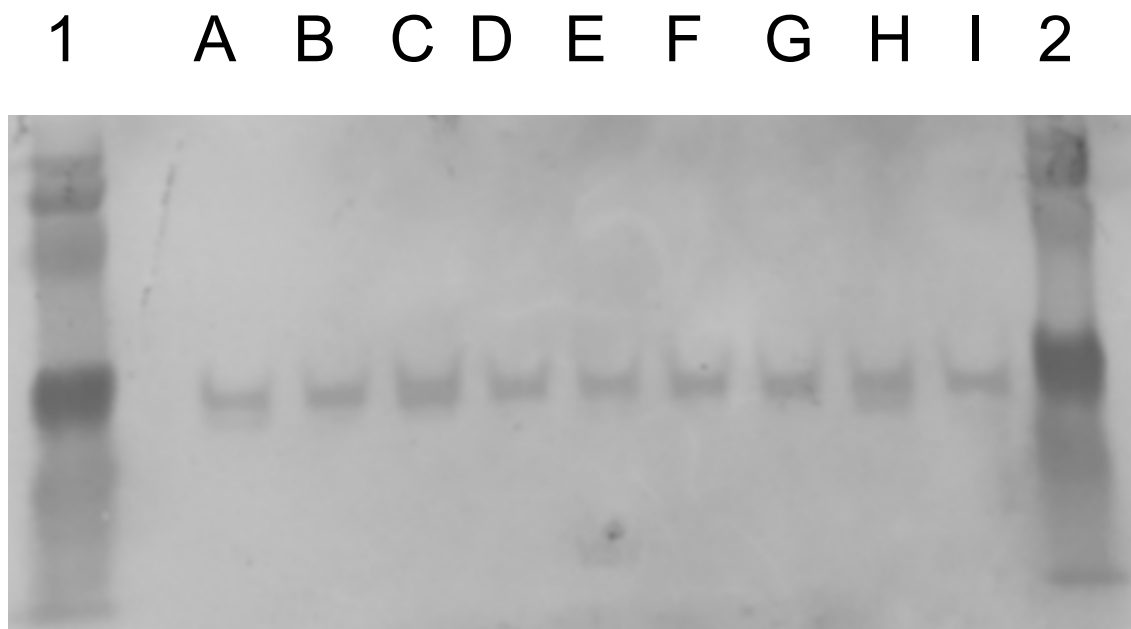


**Figure 6. Western blot of purified RihC derivatives.** Purified RihC and RihC derivatives were size-fractionated by SDS-PAGE, transferred to PVDF membranes and probed with Anti-His(C-term)-AP Alkaline Phosphatase-conjugated antibody. The lanes were loaded as follows: 1) Kaleidoscope standard, 2) unstained Kaleidoscope standard, A) RihC, B) D14A, C) D15A, D) F164A, E) R222A, F) H233A, G) D234A, H) L241A, and I) V242A.

**Table 3. Hydrolysis velocities of RihC and derivatives of uridine and inosine.**

Mutant	Uridine <sup>a</sup>	Inosine <sup>a,b</sup>
Wild type	12.9	8.72
14	0.23	ND
15	0.12	ND
164	0.21	ND
222	2.42	ND
233	3.59	0.15
234	0.22	ND
241	3.09	ND
242	9.71	ND

<sup>a</sup>  $\mu\text{mol}/\text{min}/\text{mg}$ <sup>b</sup>ND: not determined

## CHAPTER IV: DISCUSSION

IU-NHs are a class of enzymes that catalyze hydrolysis of both pyrimidines and purines to produce the sugar and the nitrogenous base (11). *E. coli* produces RihC, which has been speculated to be part of the nucleoside salvage pathway and has the characteristic N-terminus of IU-NHs (1). Previous studies have shown that RihC has many features and functions in common with *C. fasciculata*'s IU-NH, the archetype enzyme for the class (22, 26-28). Hunt *et al.* demonstrated similar transition states showing the distance between nucleophile and substrate should be greater than 2.35 Å (26). However, the mechanism of hydrolysis as performed by RihC is not completely known. It is postulated that protonation or hydrogen bonding likely occurs at O2. While the isotope effect is similar to IU-NH, RihC differs at 5'-hydroxymethyl group showing no change in the 5'-hydroxy environment (26). In spite of these differences, parallels to common residues can be made to investigate the mechanism of hydrolysis.

The active site of RihC is not open to solvent but has an ordered water molecule present. Also, RihC catalyzes an irreversible reaction, since the equilibrium constant is 45 M for inosine, at a pH optimum of 7.5 (28). This same study indicated interactions at ribosyl 2' and 3' hydroxyls are required. Nitrogen at position 7 of purines and position 3 of pyrimidines are required for hydrolysis (28). Critical residues in the active site have been predicted *in silico* (29). The residues predicted to be in the catalytic site were Asp10, Asn165, and His233. Additionally, Asp14, Asp15, Asp234, and Ile121 compose the active site. Farone *et al.* (29) proposed that His233 protonates purine N7 or pyrimidine N3 of the leaving group. The  $P_{\text{value}}$  of 0.000 provided the authors confidence in the conclusions of the study. Arivett *et al.* (28) showed a requirement for N3 for



pyrimidines hydrolysis. However, other *in silico* modeling shows the N3 to be in a suboptimal position for hydrogen bonding by His233 (18).

This current study characterized residues previously shown to be important for the functioning of IU-NH and additional homologous residue predicted to be important. Asp14, Asp15, Phe164, Arg222, His233, Asp234, Leu241, and Val242 were changed to alanine. The effects of the substitution on the activity of the enzyme were assayed by HPLC to measure the rate of decrease in the nucleoside concentration and conversely the increase in base or sugar for uridine or inosine respectively. The results of the studies confirm the importance of the Asp14, Asp15, Phe164, and Asp234 residues for pyrimidine hydrolysis. The most intriguing is His233. Although the mutation did not greatly reduce the velocity for the pyrimidine, uridine, it greatly reduced activity toward the purine, inosine. This suggests that residues at the active site of the enzyme may have specificity for different substrates. This study highlights these amino acids as candidates for future spectroscopic structure/function studies. While the reaction mechanism of promiscuous IU-NH still remains obscure, this work contributes to the identification of a residue that is critical for the function of this enzyme.

Since the transition state of *C. fasciculata* IU-NH has been studied using multiple kinetic isotope effects (KIE), bond-energy bond-order vibrational analysis (BEBOVIB) and inhibitor bound crystallography(25), its characteristics may also be important for understanding RihC. The isotope effects seen in IU-NH of *C. fasciculata* indicate that the enzyme stabilizes an  $S_N1$ -like transition state with substantial oxocarbenium ion character. Miles *et al.* proposed three strategies to accomplish this transition and provide the 17.7 kcal/mol required to cleave the glycosidic linkage, 13.1 kcal/mol of

ribosyl activation and 4.6 kcal/mol leaving group assistance in IU-NH (22). First, protonation or hydrogen bonding to the purine leaving group activates the base. Second, the electrostatic stabilization and distortion of ribosyl groups leads to formation of a ribooxocarbenium ion. Third, a captured and activated water molecule strategically positioned is required for stabilization of the ribooxocarbenium ion (9). These strategies do take place in the non-specific nucleoside hydrolase catalyzed reactions.

The protonation of the leaving group is best understood for the purine, inosine (22). KIE of 1.3 suggest N7 protonation by complete transfer of proton prior to the transition state (12,23). His241 has been shown to be crucial in the reactivity toward turnover of purines as His241Ala leads to 2100-fold decrease in activity (22). The requirement for N7 protonation is also supported by the inability of IU-NH to hydrolyze 7-deazaadenosine, where carbon replaces N7 (12). Additionally at the transition state, KIE  $^{15}\text{N}$  indicates loss of N9 bond order requires N7 protonation. This activation of the purine leaving group contributes to the glycosidic linkage almost being cleaved at the transition state with a bond length of  $1.97 \pm 0.14 \text{ \AA}$ , likely because of decreased electron density (8,12). The process of base activation for pyrimidines is less clear.

The remaining two chemical strategies involve the sugar. Since IU-NH is able to hydrolyze *p*-nitrophenyl  $\beta$ -D-ribofuranoside, indicating that activation of the nucleic base leaving group is a minor contributor to enzyme activity, these characteristics of the transition state are of greater importance than the previously discussed leaving group protonation (26). The formation of the ribooxocarbenium ion is crucial for the reaction to proceed. The electrostatic stabilization and distortion to form the ion are achieved with multiple interactions primarily with the 2'-, 3'-, and 5'- hydroxyls. Additionally, an

enzyme-directed attacking oxygen nucleophile with low bond order to the target C1' are all coordinated with the  $\text{Ca}^{2+}$  (22,25,27). Studies with iminoribitol inhibitors have been used to demonstrate the ribooxocarbenium ion transition state (9,15). These transition features have become hallmarks of the non-specific nucleoside hydrolases.

The transition state of RihC of *E. coli* has also been characterized in similar ways as IU-NH of *C. fasciculata* (28,29). RihC, like the *C. fasciculata* enzyme, forms a ribooxocarbenium ion, protonates or forms a hydrogen bond to O2 to activate the heterocyclic base, possesses an almost broken C-N glycosidic bond, and exhibits scant bond formation to the attacking nucleophile (29). Also, RihC has also been shown to be unable to hydrolyze substrates lacking 2'- and 3'- hydroxyls, while exhibiting a 500-fold decrease in activity toward erythrouridine, which lacks the C5' hydroxymethyl group (28). The apparent contradiction of studies by Hunt *et al.* with regard to the C5' hydroxymethyl may result from the difficulty in measuring the long distance KIE. The similar transition states of IU-NH and RihC provides support for the relevance of RihC studies based on homology with IU-NH.

The results of this study on RihC recapitulated many experiments for IU-NH, namely the importance for the aspartic acids at positions 14 and 15 for both enzymes and 242/234 (*C. fasciculata*/*E. coli*), with similar results. The greater than 50-fold reduction in hydrolysis of uridine for RihC underscores the importance of these residues for the reaction catalyzed by the non-specific nucleoside hydrolases. Asp14 is suggested to interact with the 2'-hydroxyl. Asp15 is positioned to coordinate the calcium ion required to be present for proper enzyme function because of its interactions with the 2'- and 3'- hydroxyls as well as ordering the  $\text{H}_2\text{O}$  nucleophile for its attack on the C1' of the

glycosidic bond. The Asp234 also had a significant decrease in activity, a similar result to that seen with the analogous residue in IU-NH, Asp242. In IU-NH, this residue interacts with both the  $\text{Ca}^{2+}$  and the 3'-hydroxyl. All of these residues of RihC, based on the well-characterized IU-NH, will contribute to the binding of the sugar group and stabilization of the ribooxocarbenium ion.

Additional RihC residues investigated in this study also resulted in significant decreases in the enzymatic activity. Phenylalanine 164 and histidine 233 both decreased the reactivity but do not appear to act upon the sugar based on crystal structure of IU-NH. His233 is interesting because of the discrimination between purine/pyrimidine base turnover. The likely mechanism is similar to IU-NH His241. The IU-NH H241A site-directed mutant showed the same purine/pyrimidine discrimination as RihC H233A and appears to be important in N7 protonation. So it is likely that RihC H233A is important for base activation by the same mechanism as IU-NH. Interestingly, the analogous residue for RihC Phe164 in IU-NH, Phe167, has not been investigated even though Asn168 has been shown to be an important residue for inhibitor binding. Phe167 is a hydrophobic residue that may be important in producing a hydrophobic pocket leading to distention of the glycosidic bond. Since, a catalytic triad of Tyr223, Tyr227 and His233 of *C. fasciculata* are expected to be out of reach to effect the activation of pyrimidine base, it may be a possibility that Phe167 is responsible for catalysis of pyrimidines, as His233 is responsible for catalysis of purines. More studies need to be done to support this possibility.

In addition to RihC, *E. coli* produces two other NHs. RihA and RihB are both pyrimidine specific, and the role of the three hydrolases in the bacterium is unclear, as

shown by the normal growth of an *E. coli* mutant lacking all three of the NH genes (1). One suggestion for the redundancy of these enzymes is that they have specialized roles in the cell, such as the degradation of modified nucleosides such as are found in tRNA (19). Although the activity of RihC for a number of substrates has already been tested, these were primarily to assess the role of structural features for enzyme activity (28), and future studies could explore the activity of these enzymes for specialized cellular nucleosides.

Besides serving as targets for microorganism-specific treatments, NHs also have therapeutic potential for solid tumors. Treatment of cancerous cells with nucleoside chemotherapeutic agents, such as 5-fluorouracil (5-FU), results in uptake by the rapidly dividing cells which convert the 5-FU to 5-fluorodeoxyuridine monophosphate. This product blocks the enzyme thymidylate synthase, interrupting thymidine synthesis, and ultimately DNA replication and the growth of the tumor cells. However, some human cells inefficiently convert the 5-FU to the inhibitor. By delivering a gene with the ability to convert 5-FU more efficiently into solid tumors through viral vectors, the tumors become more sensitive to the treatment, while the surrounding normal cells remain more resistant to the effects of the chemotherapeutic agent (19). The identification of nucleoside hydrolases with the capability to convert the 5-FU more efficiently will improve these targeted therapies. Testing the activity of the RihC and mutant proteins for chemotherapeutic nucleosides could not only help identify another potential enzyme for such treatment, but also help to determine amino acids important for this targeted activity.

## REFERENCES

1. **Petersen, C., and L. B. Moller.** 2001. The RihA, RihB, and RihC Ribonucleoside Hydrolases of *Escherichia coli*. Substrate specificity, gene expression, and regulation. *J Biol Chem* **276**:884-894.
2. **Hansen, M. R., and G. Dandanell.** 2005. Purification and characterization of RihC, a xanthosine-inosine-uridine-adenosine-preferring hydrolase from *Salmonella enterica* serovar Typhimurium. *Biochim.Biophys. Acta* **1723**:55-62.
3. **Kurtz, J. E., F. Exinger, P. Erbs, and R. Jund.** 2002. The URH1 uridine ribohydrolase of *Saccharomyces cerevisiae*. *Curr Genet* **41**:132-141.
4. **Koszalka, G. W., and T. A. Krenitsky.** 1979. Nucleosidases from *Leishmania donovani*. Pyrimidine ribonucleosidase, purine ribonucleosidase, and a novel purine 2'-deoxyribonucleosidase. *J Biol Chem* **254**:8185-8193.
5. **Miller, R. L., C. L. Sabourin, T. A. Krenitsky, R. L. Berens, and J. J. Marr.** 1984. Nucleoside hydrolases from *Trypanosoma cruzi*. *J Biol Chem* **259**:5073-5077.
6. **Ribeiro, J. M., and J. G. Valenzuela.** 2003. The salivary purine nucleosidase of the mosquito, *Aedes aegypti*. *Insect Biochem Mol Biol* **33**:13-22.
7. **Versees, W., E. Van Holsbeke, S. De Vos, K. Decanniere, I. Zegers, and J. Steyaert.** 2003. Cloning, preliminary characterization and crystallization of nucleoside hydrolases from *Caenorhabditis elegans* and *Campylobacter jejuni*. *Acta Crystallogr D Biol Crystallogr* **59**:1087-1089.
8. **Versees, W., and J. Steyaert.** 2003. Catalysis by nucleoside hydrolases. *Curr Opin Struct Biol* **13**:731-738.
9. **Miles, R. W., P. C. Tyler, G. B. Evans, R. H. Furneaux, D. W. Parkin, and V. L. Schramm.** 1999. Iminoribitol transition state analogue inhibitors of protozoan nucleoside hydrolases. *Biochemistry* **38**:13147-13154.
10. **Belenky, P., F. G. Racette, K. L. Bogan, J. M. McClure, J. S. Smith, and C. Brenner.** 2007. Nicotinamide riboside promotes Sir2 silencing and extends lifespan via Nrk and Urh1/Pnp1/Meu1 pathways to NAD<sup>+</sup>. *Cell* **129**:473-484.
11. **Parkin, D. W., B. A. Horenstein, D. R. Abdulah, B. Estupinan, and V. L. Schramm.** 1991. Nucleoside hydrolase from *Crithidia fasciculata*. Metabolic role, purification, specificity, and kinetic mechanism. *J Biol Chem* **266**:20658-20665.

12. **Todd, S. J., A. J. G. Moir, M. J. Johnson, and A. Moir.** 2003. Genes of *Bacillus cereus* and *Bacillus anthracis* encoding proteins of the exosporium. *J Bacteriol* **185**:3373-3378.
13. **Schramm, V. L., B. A. Horenstein, and P. C. Kline.** 1994. Transition state analysis and inhibitor design for enzymatic reactions. *J Biol Chem* **269**:18259-18262.
14. **Rugemalila, J. B., O. A. T. Ogundahunsi, T. T. Stedman, and W. L. Kilama.** 2007. Multilateral initiative on malaria: justification, evolution, achievements, challenges, opportunities, and future plans. *Am J Trop Med Hyg* **77**:296-302.
15. **Horenstein, B. A., and V. L. Schramm.** 1993. Electronic nature of the transition state for nucleoside hydrolase. A blueprint for inhibitor design. *Biochemistry* **32**:7089-7097.
16. **Horenstein, B. A., and V. L. Schramm.** 1993. Correlation of the molecular electrostatic potential surface of an enzymatic transition state with novel transition-state inhibitors. *Biochemistry* **32**:9917-9925.
17. **Schramm, V. L.** 1997. Enzymatic N-riboside scission in RNA and RNA precursors. *Curr Opin Chem Biol* **1**:323-331.
18. **Iovane, E., B. Giabbai, L. Muzzolini, V. Matafora, A. Fornili, C. Minici, F. Giannese, and M. Degano.** 2008. Structural basis for substrate specificity in group I nucleoside hydrolases. *Biochemistry* **47**:4418-4426.
19. **Giabbai, B., and M. Degano.** 2004. Crystal structure to 1.7 Å of the *Escherichia coli* pyrimidine nucleoside hydrolase YeiK, a novel candidate for cancer gene therapy. *Structure* **12**:739-749.
20. **Estupinan, B., and V. L. Schramm.** 1994. Guanosine-inosine-preferring nucleoside N-glycohydrolase from *Crithidia fasciculata*. *J Biol Chem* **269**:23068-23073.
21. **Alonso, G., P. Guevara, and J. L. Ramirez.** 1992. Trypanosomatidae codon usage and GC distribution. *Mem Inst Oswaldo Cruz* **87**:517-523.
22. **Gopaul, D. N., S. L. Meyer, M. Degano, J. C. Sacchettini, and V. L. Schramm.** 1996. Inosine-Uridine Nucleoside Hydrolase from *Crithidia fasciculata*. Genetic characterization, crystallization, and identification of histidine 241 as a catalytic site residue. *Biochemistry* **35**:5963-5970.
23. **Horenstein, B. A., D. W. Parkin, B. Estupinan, and V. L. Schramm.** 1991. Transition-state analysis of nucleoside hydrolase from *Crithidia fasciculata*. *Biochemistry* **30**:10788-10795.

24. **Shi, W., V. L. Schramm, and S. C. Almo.** 1999. Nucleoside hydrolase from *Leishmania major*. Cloning, expression, catalytic properties, transition state inhibitors, and the 2.5-Å crystal structure. *J Biol Chem* **274**:21114-21120.
25. **Degano, M., S. C. Almo, J. C. Sacchettini, and V. L. Schramm.** 1998. Trypanosomal nucleoside hydrolase. A novel mechanism from the structure with a transition-state inhibitor. *Biochemistry* **37**:6277-6285.
26. **Hunt, C., N. Gillani, A. Farone, M. Rezaei, and P. C. Kline.** 2005. Kinetic isotope effects of nucleoside hydrolase from *Escherichia coli*. *BBA-Proteins & Proteomics* **1751**:140-149.
27. **Degano, M., D. N. Gopaul, G. Scapin, V. L. Schramm, and J. C. Sacchettini.** 1996. Three-dimensional structure of the inosine-uridine nucleoside N-ribohydrolase from *Crithidia fasciculata*. *Biochemistry* **35**:5971-5981.
28. **Arivett, B., M. Farone, R. Masiragani, A. Burden, S. Judge, A. Osinloye, C. Minici, M. Degano, M. Robinson, and P. Kline.** 2014. Characterization of inosine-uridine nucleoside hydrolase (RihC) from *Escherichia coli*. *BBA-Proteins and Proteomics* **1844**:656-662.
29. **Farone, A., M. Farone, P. Kline, T. Quinn, and Z. Sinkala.** 2010. A Practical Approach for computing the active site of the ribonucleoside hydrolase of *E. coli* encoded by rihC, p. 437-443, *Advances in Computational Biology*. Springer.



**APPENDICES**

**APPENDIX A****Buffers and Solutions****A. 0.5 M EDTA (per Liter)**

Na <sub>2</sub> EDTA·2H <sub>2</sub> O	186.1 g
Adjust pH to 8.0 with 10 M NaOH	

**B. Luria-Bertani (LB) Broth (per Liter)**

Tryptone	10 g
Yeast extract	5 g
NaCl	10 g

**C. LB Agar (per Liter)**

Tryptone	10 g
Yeast extract	5 g
NaCl	10 g
Agar	20 g

**D. LB-Kanamycin/Chloremphenicol (per Liter)**

Tryptone	10 g
Yeast extract	5 g
NaCl	10 g
Agar	20 g

After autoclaving, cool media to 50°C and add  
5 ml of 200X Kanamycin and Chloremphenicol

**E. TBS pH 7.2 (per Liter)**

Tris	2.43 g
NaCl	8.18 g

**F. TE Buffer**

10 mM Tris.Cl pH 7.4  
1 mM EDTA

**G. 200X Kanamycin (per Liter)**

Kanamycin Sulfate	10 g
in distilled H <sub>2</sub> O	

**H. 1000X Chloremphenicol (per Liter)**

Chloremphenicol in ethanol	34 g
----------------------------	------

**I. Stratagene dNTP mix**

25 mM dATP  
 25 mM dTTP  
 25 mM dCTP  
 25 mM dGTP

**J. SOC Broth (per Liter)**

Tryptone	20 g
Yeast extract	5 g
NaCl	0.5 g

*Q.S.* 1 liter Autoclave  
 Add 10 ml of sterilized 1 M MgCl<sub>2</sub> and  
 10 ml sterilized 1 M MgSO<sub>4</sub> prior to use  
 Add 1 ml 2 M sterilized glucose to final  
 volume 100 ml filter sterilize

**K. TAE Buffer (per Liter)**

50X stock solution, pH 8.5	
Tris base	242 g
Glacial acetic acid	57.1 mL
Na <sub>2</sub> EDTA·2H <sub>2</sub> O	
1X working solution:	
40 mM Tris Acetate	
2 mM EDTA	

**L. 6X PCR loading buffer (per Liter)**

0.25% (w/v) Bromophenol blue	50 mg
0.25% (w/v) Xylene cyanol FF	25 mg
40.0% (w/v) Sucrose	4 g

**M. P1 Buffer**

50 mM Tris·CL, pH 8.0,  
10 mM EDTA  
100 µg/ml RNase A

**N. P2 Buffer**

200 mM NaOH  
1% SDS (w/v)

**O. N3 Buffer**

Proprietary formulation (Qiagen Inc., Valencia, CA)

**P. PB Buffer**

Proprietary formulation (Qiagen Inc., Valencia, CA)

**Q. PE Buffer**

Proprietary formulation (Qiagen Inc., Valencia, CA)

**R. 10X Reaction Buffer**

100 mM KCl  
100 mM (NH<sub>4</sub>)<sub>2</sub>SO<sub>4</sub>  
200 mM Tris-HCl (pH 8.8)  
20 mM MgSO<sub>4</sub>  
1% (v/v) Triton® X-100  
1 mg/ml nuclease-free bovine serum albumin

**S. His Column Elution Buffer pH 8.0 (per Liter)**

NaPO <sub>4</sub>	3.45 g
NaCL	29.2 g
Imidazole	17.0 g

**T. His Column Equilibration/Wash Buffer pH 8.0 (per Liter)**

NaPO <sub>4</sub>	6.9 g
NaCL	29.2 g
Imidazole	3.4 g

**U. TBST (per Liter)**

TBS	999 mL
Tween-20	1 mL

**V. NZY Broth (per Liter)**

NaCl	5 g
MgSO <sub>4</sub> ·7H <sub>2</sub> O	2 g
Yeast extract	5 g
NZ amine	10 g

**W. Phosphate-Buffered Saline, pH 7.3**

137 mM NaCl
2.7 mM KCl
4.3 mM Na <sub>2</sub> HPO <sub>4</sub> ·7H <sub>2</sub> O
1.4 mM KH <sub>2</sub> PO <sub>4</sub>

**X. Blocking Buffer**

PBS
5% Tryptone (w/v)

**Y. Dilution Buffer**

TBST
1% Tryptone (w/v)

**Z. Alkaline Phosphatase Buffer, pH 9.5**

100 mM diethanolamine
100 mM NaCl
5 mM MgCl <sub>2</sub>

**AA. Bromochloroindolyl Phosphate Stock Solution (per Liter)**

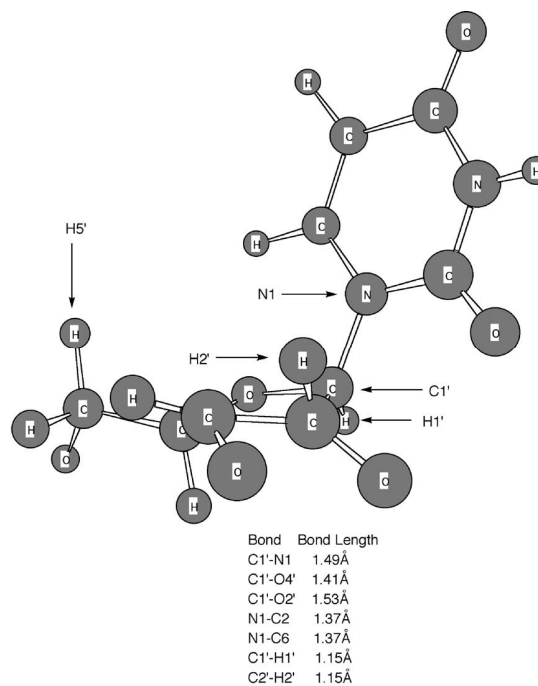
Bromochloroindolyl phosphate	50 g
in 100% (v/v) dimethylformamide	

**BB. Nitro Blue Tetrazolium Stock Solution (per Liter)**

Nitro Blue Tetrazolium	50 g
in 70% (v/v) dimethylformamide	

## APPENDIX B

### Ground State of Uridine



Ground state of uridine (hydroxyl hydrogens omitted). The sites of isotopic substitution are indicated. The structure was based upon the crystal structure of Green and coworkers, followed by energy minimization using Spartan 5 and Gaussian 98W. The bond lengths listed are after energy minimization. The conformation of the ribose ring is C3V-endo, while the conformation about the glycosidic bond is anti (26).

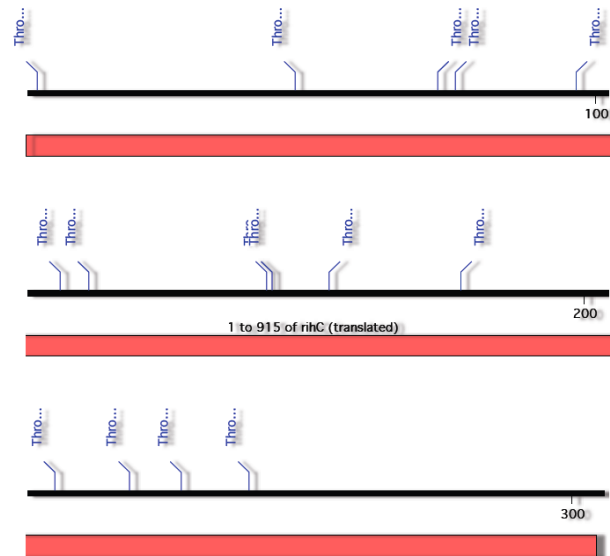
## APPENDIX C

*In silico* Digestion of RihC

<b>Name</b>	<b># Cuts</b>	<b>Location</b>					
Acid Hydrolase	2						
		10	169				
AspN	25						
		89	108	135	138	157	168
		174	185	188	198	233	235
		244	251	269	271	273	285
		387					
Chymotrypsin	19						
		6	24	55	56	89	91
		104	142	164	177	200	218
		221	240	247	253	262	292
		295					
LysC	7						
		44	97	140	212	250	277
		290					
Thrombin	15						
		2	47	72	75	96	108
		113	144	145	155	178	209
		222	231	243			
Trypsin	22						
		2	44	47	72	75	96
		97	108	113	140	144	145
		155	178	209	212	222	231
		243	250	277	290		
TrypK	7						
		44	97	140	212	250	277
		290					
TrypR	15						
		2	47	72	75	96	108
		113	144	145	155	178	209
		222	231	243			
Enterokinase	0						
Tev protease	0						

## APPENDIX D

## Thrombin Digestion of RihC



*In silico* thrombin digest of *E. coli* RihC. The translated primary sequence of *rihC* was subjected to analysis to determine potential digestion fragments when enzymatically digested with thrombin. pET28 vectors allow for thrombin digestion to remove N-terminal poly-histidine tag. Prepared Using MacVector 11.1.



## APPENDIX E

### RihC Characteristics and Amino Acid Composition

Amino Acid Composition:

Non-polar:	No.	Percent
A	39	12.79
V	24	7.87
L	36	11.80
I	17	5.57
P	20	6.56
M	9	2.95
F	12	3.93
W	3	0.98

Polar:	No.	Percent
G	22	7.21
S	13	4.26
T	17	5.57
C	8	2.62
Y	4	1.31
N	11	3.61
Q	11	3.61

Acidic:	No.	Percent
D	17	5.57
E	13	4.26

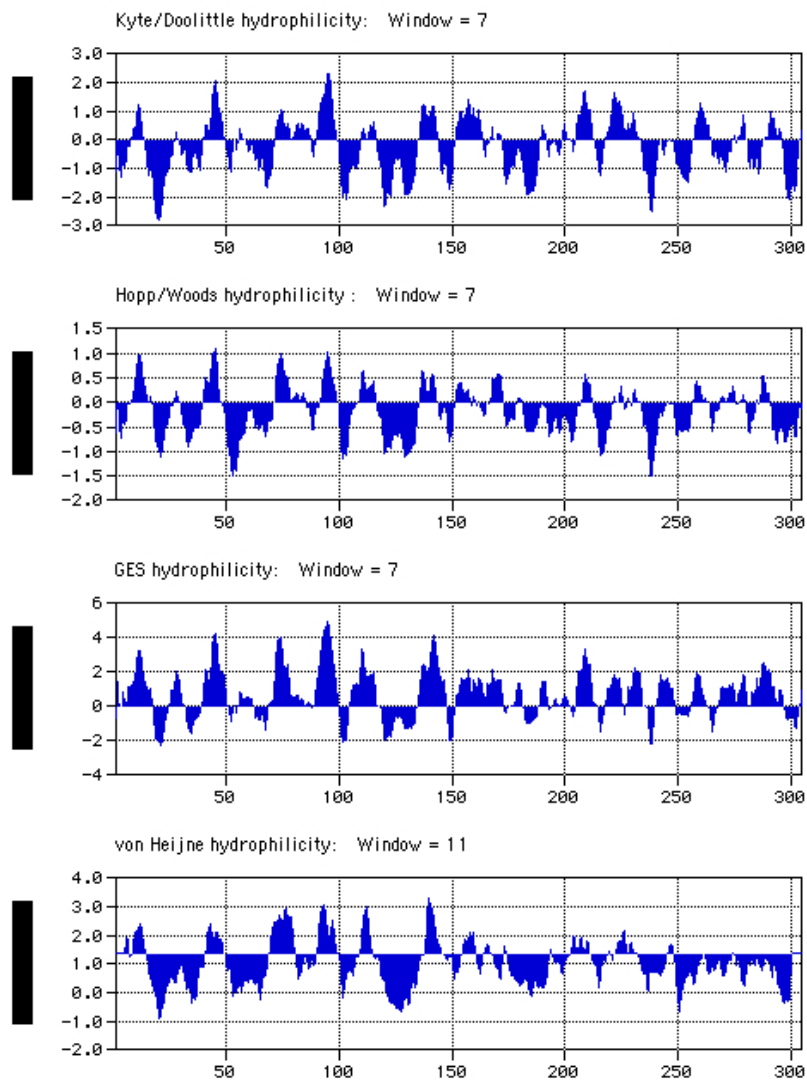
Basic:	No.	Percent
K	7	2.30
R	15	4.92
H	6	1.97

Calculated Molecular Weight = 32558.67

Estimated pI = 5.08

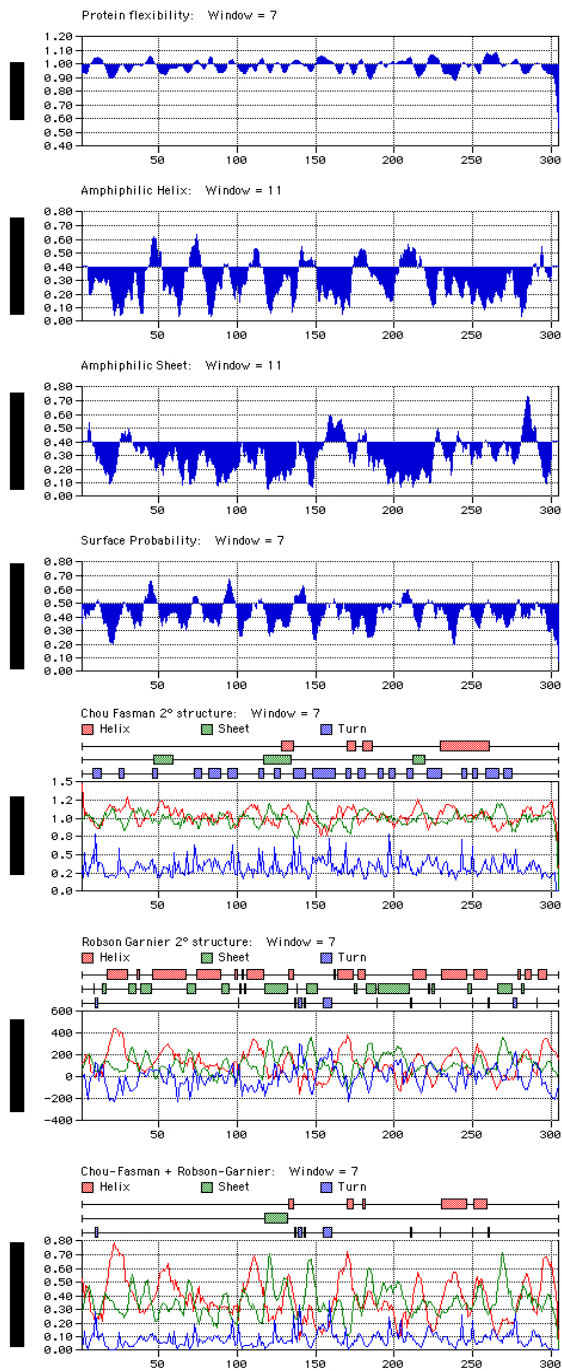
## APPENDIX F

## Estimations of RihC Hydrophilicity

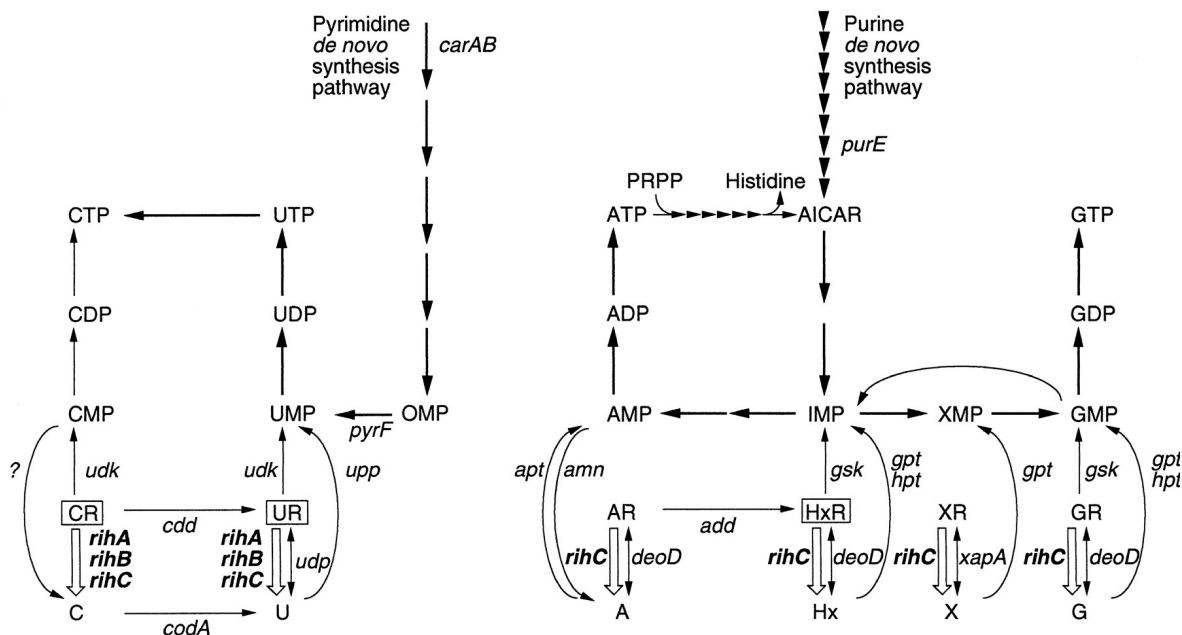


## APPENDIX G

## Structural Algorithms for RihC



## APPENDIX H

*E. coli* Purine and Pyrimidine Pathway

Pathway of pyrimidine and purine metabolism in *E. coli*. Ribonucleoside hydrolases; RihA, RihB and RihC, reactions are shown with open arrows. Nucleosides utilized are shown. C, cytosine; CR, cytidine; U, uracil; UR, uridine; A, adenine; AR, adenosine; Hx, hypoxanthine; HxR, inosine; X, xanthine; XR, xanthosine; G, guanine; GR, guanosine; PRPP, 5-phosphoribosyl-a-1-pyrophosphate; AICAR, 5-amino-4-imidazolecarboxamide ribonucleotide. (1)

## APPENDIX I

## Novagen pET-28a-c (+) Vector Technical Bulletin



## pET-28a-c(+) Vectors

TB074 12/98

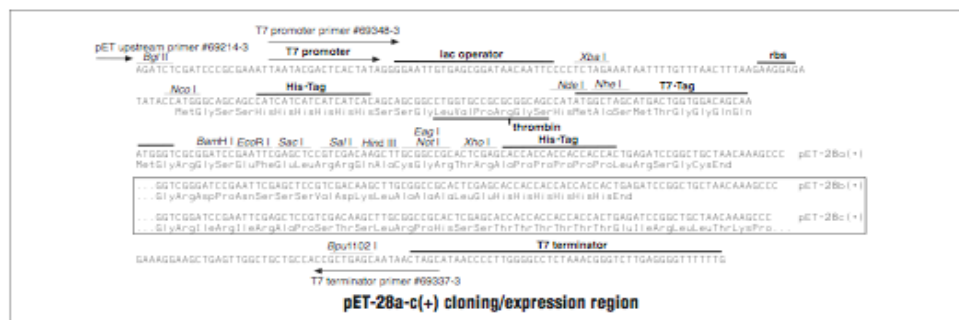
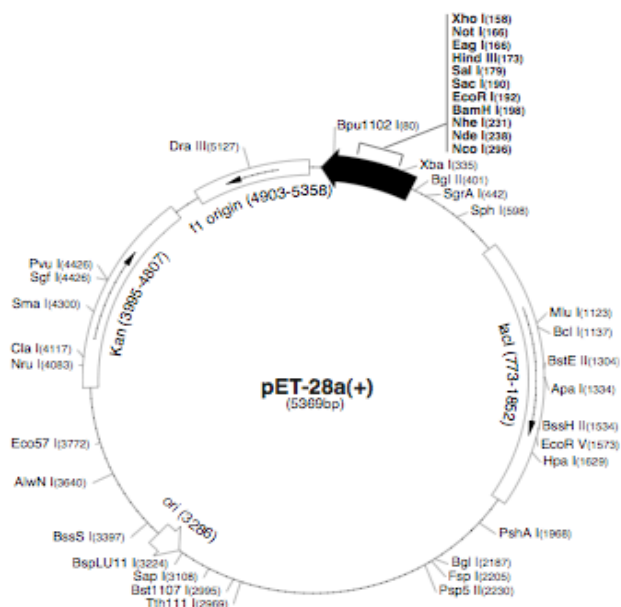
	Cat. No.
pET-28a DNA	69864-3
pET-28b DNA	69865-3
pET-28c DNA	69866-3

The pET-28a-c(+) vectors carry an N-terminal His•Tag<sup>®</sup>/thrombin/T7•Tag<sup>®</sup> configuration plus an optional C-terminal His•Tag sequence. Unique sites are shown on the circle map. Note that the sequence is numbered by the pBR322 convention, so the T7 expression region is reversed on the circular map. The cloning/expression region of the coding strand transcribed by T7 RNA polymerase is shown below. The fl origin is oriented so that infection with helper phage will produce virions containing single-stranded DNA that corresponds to the coding strand. Therefore, single-stranded sequencing should be performed using the T7 terminator primer (Cat. No. 69337-3).

## pET-28a(+) sequence landmarks

T7 promoter	370-386
T7 transcription start	369
His•Tag coding sequence	270-287
T7•Tag coding sequence	207-239
Multiple cloning sites ( <i>Bam</i> H I - <i>Xho</i> I)	158-203
His•Tag coding sequence	140-157
T7 terminator	26-72
<i>lacI</i> coding sequence	773-1852
pBR322 origin	3286
Kan coding sequence	3995-4807
fl origin	4903-5358

The maps for pET-28b(+) and pET-28c(+) are the same as pET-28a(+) (shown) with the following exceptions: pET-28b(+) is a 5368bp plasmid; subtract 1bp from each site beyond *Bam*H I at 198. pET-28c(+) is a 5367bp plasmid; subtract 2bp from each site beyond *Bam*H I at 198.



Novagen • ORDERING 800-526-7319 • TECHNICAL SUPPORT 800-207-0144